Modeling, Optimization, and Experimentation of the ParaGripper for In-Hand Manipulation Without Parasitic Rotation

Huan Liu, Longhai Zhao, Bruno Siciliano, and Fanny Ficuciello

***Abstract*—Recently, underactuated robotic hands have been exploited for dexterous in-hand manipulation, after having been proven efficient in performing versatile adaptive grasps. However, the reported in-hand manipulation skills are usually associated with parasitic motion, which may complicate control and application of the hand. This paper presents the modeling, optimization and experimentation of the ParaGripper, an underactuated gripper capable of performing in-hand manipulation without parasitic rotation. The underactuated finger uses two serially connected parallelograms to ensure pure translation of the fingertips. If the object remains stationary within the fingertips, the gripper can translate the object without parasitic rotation. The kinematics and kinetostatics of the hand–object system are derived and the manipulation workspace is optimized. The ParaGripper is designed and fabricated according to suitable optimal parameters. Experiments show that the ParaGripper could perform non-parasitic in-hand manipulation and versatile adaptive grasps.**

***Index Terms*—Grippers and other end-effectors, dexterous manipulation, mechanism design.**

I. Introduction

THE in-hand manipulation capability of a human hand brings better accuracy, efficiency and kinematic redundancy to human hand-arm system and serves as a model for ideal robotic manipulation systems. Since the foundations of multi-finger robotic hands were laid in 1980s [1], [2], various highly-articulated hands (e.g., the JPL hand [1], the DLR hand [3], the DEXMART hand [4] and the commercial Shadow Hand) have been designed using emerging technologies. However, in-hand manipulation of objects using such hands remains a true challenge. The control strategies are usually complex, since about 20 finger joints need to be coordinated. The precise modeling of the fingers and object are required for model-based control [1], [5], while substantial training is necessary for a machine leaning-based approach [6]–[8].

Underactuated robotic hands were usually designed to perform adaptive grasps. Recently, a framework for performing in-hand manipulation by underactuated hands has been proposed [9]. This is motivated by the fact that using fewer actuators simplifies not only the design but also the control of a hand. Several grippers with in-hand manipulation capability have been designed, including the iHY hand [10], the GR2 gripper [11], the grippers for caging manipulation [12] and a single-actuator gripper [13] using the continuum differential mechanism [14]. As evidenced by the aforementioned examples, an underactuated hand can also perform in-hand manipulation if wisely designed.

The problem is that the performed in-hand manipulation is usually associated with parasitic motion, which is coupled to the independently-controlled motion(s). For example, in [9] when the object was moved from the leftmost to the rightmost of its manipulation workspace, the object was rotated approximately by one radian. For the in-hand rolling manipulation presented in [13], the object was translated simultaneously. Undesired parasitic motion might need to be compensated using a robotic arm [15]. Utilization of the in-hand manipulation skill of the hand could thus become complicated.

This research attempts to design a robotic gripper that is capable of in-hand manipulation without parasitic rotation, while the multi-grasp efficiency of the gripper is preserved by adopting an underactuated finger design. Inspired by the low-mobility parallel mechanisms (PMs) for pure translation [16]–[18], we developed the ParaGripper, an underactuated gripper capable of pure translational in-hand manipulation, as shown in Fig. 1. Each finger of the gripper uses two serially connected parallelograms, which prevail in PMs, to ensure pure translation of the fingertip. If the fingertips are suitably designed so that the object remains stationary within the fingertips, the object can be manipulated without parasitic rotation.

The paper elaborates the schematic, modeling, optimization and experimentation of the ParaGripper, and is organized as follows. Section II describes the schematic and modeling of the gripper while Section III presents the optimization of the

Manuscript received September 9, 2019; accepted January 22, 2020. Date of publication February 17, 2020; date of current version March 2, 2020. This research has been partially funded by the POR FESR 2014-2020 Italian National programme within BARTOLO project (CUP B41C17000090007) and by the PNR 2015-2020 Italian National programme within PROSCAN project (CUP UNINA: E26C18000170005). This letter was recommended for publication by Associate Editor M. R. Dogar and Editor H. Liu upon evaluation of the reviewers' comments. *(Corresponding author: Fanny Ficuciello.)*

Huan Liu, Bruno Siciliano, and Fanny Ficuciello are with the Interdepartmental Center for Advances in Robotic Surgery (ICAROS Center), University of Naples Federico II, 80138 Naples, Italy (e-mail: hzauliuhuan@gmail.com; bruno.siciliano@unina.it; fanny.ficuciello@unina.it).

Longhai Zhao is with the School of Mechanical Engineering, Shanghai Jiao Tong University, Shanghai 200240, China (e-mail: fhqdxitx1988@sjtu.edu.cn).

This article has supplementary downloadable material available at http://ieeexplore.ieee.org, provided by the authors.

Digital Object Identifier 10.1109/LRA.2020.2974419

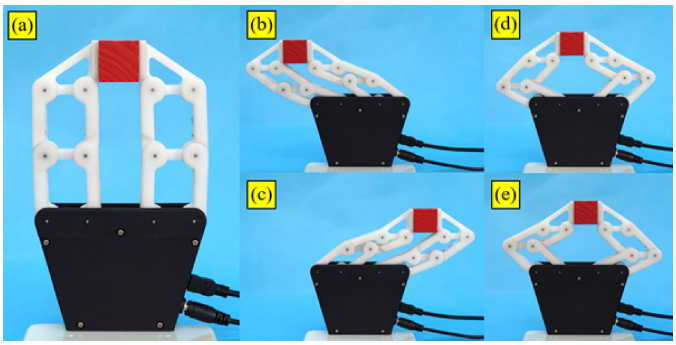

Fig. 1. The developed ParaGripper manipulating a 25 mm cube. (a)∼(e) show five typical configurations.

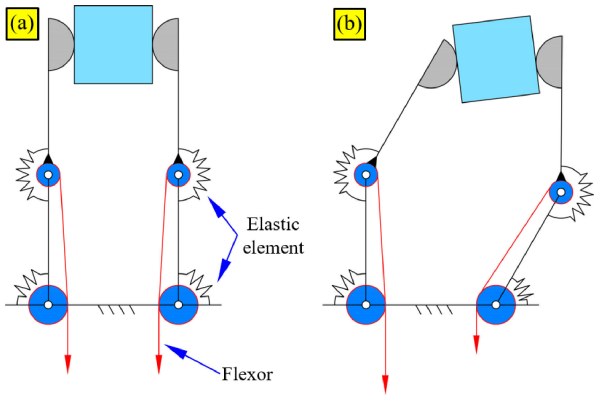

Fig. 2. Schematic of conventional underactuated finger design for in-hand manipulation.

manipulation workspace. Experimental results are reported in Section IV, while the conclusions and future directions are summarized in Section V.

II. Schematic and Modeling of the Gripper

This section presents the schematic and modeling of the ParaGripper for 2-degree-of-freedom (DoF) translational in-hand manipulation.

A. Schematic Design of the Gripper

Fig. 2 shows the schematic of a gripper with the widely-adopted underactuated finger design as in [9], [19], [20]. Each finger has two joints driven by one tendon. Each joint has an elastic element (e.g., a torsional spring) to extend it.

By pulling the tendons, the hand can perform prehensile grasp on an object using both the proximal and distal phalanges. The gripper can also pinch an object by its fingertips, as shown in Fig. 2(a), in which a cube is pinched. By continuing to pull the tendon(s), the cube is suitably manipulated within the fingertips. For example, by pulling the tendon of the left finger, the object is pushed rightward as shown in Fig. 2(b). Due to the compliance of the underactuated finger design, the right fingertip is pushed rightward accordingly. As the fingertip rolls on the object, the object is rotated with respect to the base. This in-hand manipulation capability has been demonstrated by the iHY hand [10].

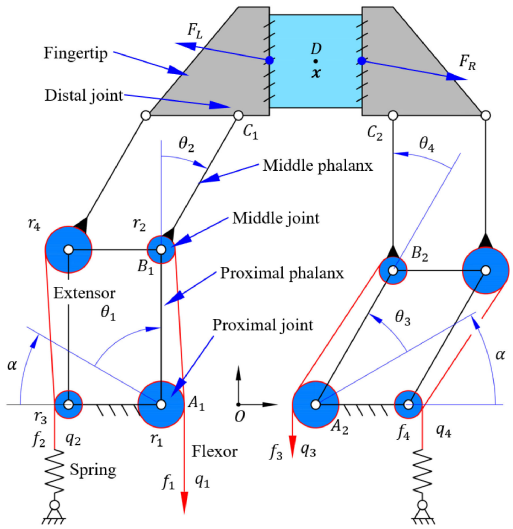

Fig. 3. Schematic of the ParaGripper for non-parasitic in-hand manipulation.

If the translation of the object is considered as the desired in-hand manipulation motion, this motion is always associated with a coupled rotation, which is similar to the parasitic motion of lower motility PMs [21]. This undesired parasitic motion may complicate the control of a hand–arm system for desired manipulation task. Compensation motion by a robot arm may thus be needed [15] to cancel the parasitic motion.

Parasitic motion has been investigated in PM research, as it is considered as a major drawback of lower mobility PMs. The parallelogram is an elementary component for synthesis of PMs for pure translation, as it keeps the coupler link remain parallel to the base link [18]. Applications of a parallelogram for pure translation can be found in the Delta robot and other pure 3 T mechanisms (T denotes a translation DoF) [16]–[18].

Some robotic grippers, such as the RG2 Gripper (OnRobot A/S, Denmark), use one parallelogram for each finger to ensure a parallel fingertip pinch grasp. Particularly, the SARAH Hand [22] and the commercial Robotiq 3-Finger Gripper (Robotiq Inc., Canada) use two serially connected parallelograms for each finger. Thus the fingertips remain parallel to each other in pinch grasps, which is the same as our design. However, it is not reported whether these hands have been optimized and exploited for in-hand manipulation.

Inspired by the similarity between in-hand manipulation and PMs [23], we propose the schematic of the ParaGripper for 2-DoF pure translation, as shown in Fig. 3. The ParaGripper has two fingers and each finger is composed of two serially connected parallelograms. As with the adopted parallelograms, the fingertips maintain their orientation during flexion/extension of the fingers. If the object remains stationary within the fingertips, i.e., the object is not rotated or slid by the fingertips, the gripper and the pinched object form a stable closed-loop kinematic chain. Thus, the orientation of the object will be maintained during in-hand manipulation.

Fingertips should be designed according to objects to prevent sliding and rotation during in-hand manipulation. For example, parallel fingertips are adopted for the manipulation of a cube,

as shown in Fig. 3. It is analyzed in Section III-A how the sliding and rotation of the cube can be avoided. In Section IV-B, prismatic fingertips are adopted to manipulate cylindrical objects. A universal fingertip design that adapts to various objects is of our interest. Integration of a pin array [24] or a granular structure [25] with variable stiffness, which conforms to different objects at low stiffness and engages firm stationary contact with the objects at high stiffness, could be a possible solution.

The underactuated finger design shown in Fig. 3 is modified from typical tendon-driven fingers [19], [20], except that the flexor and the extensor of each finger are arranged to the crankers and rockers of the parallelograms separately. The extensors are connected to tensional springs so that the fingers are extended. Since the radii of the pulley are designed as $r_4 > r_3$ and $r_1 > r_2$, the middle joints has higher stiffness than the proximal joints. Therefore, pulling the flexors will close the proximal joints first. By this design, the gripper can perform power grasp using multiple phalanges and pinch grasp using only the fingertips.

When an object is pinched by the fingertips, continuing to pull the flexors will open the proximal joints and close the middle joints, due to the designed combination of joint stiffness. If the object remains stationary within the fingertips, it will be translated in the plane without parasitic rotation.

B. Modeling of the Hand–Object System

This subsection presents the kinematic and kinetostatic modeling of the closed-loop chain formed by the ParaGripper and an object.

1) Kinematics: The schematic of the gripper is shown in Fig. 3. The position of the object, the joint angles and the tendon actuation lengths are indicated by $\mathbf{x}$, $\boldsymbol{\theta}$ and $\mathbf{q}$, respectively. Subscript R and L denote the right and left finger, respectively.

$$\mathbf{x} = \begin{bmatrix} x & y \end{bmatrix}^T \tag{1}$$

$$\boldsymbol{\theta} = \begin{bmatrix} \boldsymbol{\theta}_L | \boldsymbol{\theta}_R \end{bmatrix}^T = \begin{bmatrix} \theta_1 & \theta_2 | \theta_3 & \theta_4 \end{bmatrix}^T \tag{2}$$

$$\mathbf{q} = \begin{bmatrix} \mathbf{q}_L | \mathbf{q}_R \end{bmatrix}^T = \begin{bmatrix} q_1 & q_2 | q_3 & q_4 \end{bmatrix}^T \tag{3}$$

The tendon actuation $\mathbf{q}$ is related to the joint angles $\boldsymbol{\theta}$ by:

$$\mathbf{R}\boldsymbol{\theta} = \mathbf{q} \tag{4}$$

where $\mathbf{R}$ is the transmission matrix composed by the radii of pulleys ($r_1 \sim r_4$) in the following form:

$$\mathbf{R} = \left[\begin{array}{c|c} \mathbf{R}_L & \mathbf{0} \\ \hline \mathbf{0} & \mathbf{R}_R \end{array}\right] = \left[\begin{array}{cc|cc} r_1 & r_2 & \multicolumn{2}{c}{\multirow{2}{*}{$\mathbf{0}$}} \\ -r_3 & -r_4 & & \\ \hline \multicolumn{2}{c|}{\multirow{2}{*}{$\mathbf{0}$}} & r_1 & r_2 \\ & & -r_3 & -r_4 \end{array}\right] \tag{5}$$

The geometry of the hand–object system is subject to

$$\overrightarrow{OA_1} + \overrightarrow{A_1B_1} + \overrightarrow{B_1C_1} + \overrightarrow{C_1D} = \mathbf{x} \tag{6}$$

$$\overrightarrow{OA_2} + \overrightarrow{A_2B_2} + \overrightarrow{B_2C_2} + \overrightarrow{C_2D} = \mathbf{x} \tag{7}$$

For forward kinematics, as $\mathbf{q}$ is given, $\mathbf{x}$ and $\boldsymbol{\theta}$ can be solved from Eqn. (4), (6) and (7). For inverse kinematics, once $\mathbf{x}$ is given, $\boldsymbol{\theta}$ can be solved by Eqn. (6) and (7). Then $\mathbf{q}$ can be calculated by Eqn. (4).

2) Kinetostatics: Each finger is driven by only one tendon, hence the contact force applied on an object cannot wholly be controlled as for a fully-actuated finger. Therefore, it is necessary to analyze the contact force to assure the hand–object system maintains static equilibrium. To solve the contact force, we assume that the object remains stationary within the fingertips during manipulation. In this modeling we take the parallel fingertip and the cube shown in Fig. 3 as an example to proceed with the kinetostatic analysis.

For the left finger, the velocities of tendon actuation $\dot{\mathbf{q}}_L$ are related to the velocities of finger joints $\dot{\boldsymbol{\theta}}_L$ by

$$\mathbf{R}_L\dot{\boldsymbol{\theta}}_L = \dot{\mathbf{q}}_L \tag{8}$$

Therefore, the tensions of the tendons $\mathbf{f}_L$ and the joint torques $\boldsymbol{\tau}_L$ are related by

$$\boldsymbol{\tau}_L = \mathbf{R}_L^T\mathbf{f}_L \tag{9}$$

where $\mathbf{f}_L = [f_1, f_2]^T$. f_1 and f_2 are the tensions on the flexor and extensor, respectively. f_2 is produced by the extension spring and can be calculated by

$$f_2 = k([r_3, r_4]\,\boldsymbol{\theta}_L + l_p) \tag{10}$$

where k is the stiffness and l_p is the preload of the spring.

The Joint velocity $\dot{\boldsymbol{\theta}}_L$ and the object velocity $\dot{\mathbf{x}}$ are related by the Jacobian matrix of the left finger as

$$\dot{\mathbf{x}} = \mathbf{J}_L\dot{\boldsymbol{\theta}}_L \tag{11}$$

The Jacobian matrix can be written as:

$$\mathbf{J}_L = \begin{bmatrix} l_1\sin\theta_1' + l_2\sin\theta_2' & l_2\sin\theta_2' \\ -l_1\cos\theta_1' - l_2\cos\theta_2' & -l_2\cos\theta_2' \end{bmatrix} \tag{12}$$

where $\theta_1' = \pi - \alpha - \theta_1$ and $\theta_2' = \pi - \alpha - \theta_1 - \theta_2$.

Therefore, the joint torque $\boldsymbol{\tau}_L$ is given by

$$\boldsymbol{\tau}_L = \mathbf{J}_L^T\mathbf{F}_L \tag{13}$$

where $\mathbf{F}_L$ is the contact force applied on the left fingertip.

Combining Eqns. (9) and (13) gives the relationship between the tendon actuation force $\mathbf{f}_L$ and the contact force $\mathbf{F}_L$ of the left finger as

$$\mathbf{J}_L^T\mathbf{F}_L = \mathbf{R}_L^T\mathbf{f}_L \tag{14}$$

Similarly, for the right finger it is

$$\mathbf{J}_R^T\mathbf{F}_R = \mathbf{R}_R^T\mathbf{f}_R \tag{15}$$

where $\mathbf{F}_L = -\mathbf{F}_R$.

Given a kinematic configuration of the hand–object system, the contact forces $\mathbf{F}_L$ and $\mathbf{F}_R$, the tendon actuation forces $\mathbf{f}_L$ and $\mathbf{f}_R$ can be solved using Eqns. (14)–(15). Once the contact forces $\mathbf{F}_L$ and $\mathbf{F}_R$ are solved, it is possible to check whether sliding or rotation is prohibited, considering the contact conditions between the fingertip and the object (e.g., the contact points and friction coefficient).

III. Optimization and Design of the Gripper

This section presents the optimization of the ParaGripper toward maximal in-hand manipulation workspace.

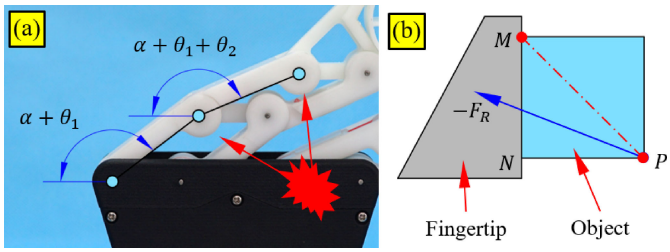

Fig. 4. (a) Constraints on joints angles to avoid the collision of the links. (b) Constraint on contact force direction to avoid rotation about point-M.

A. Formulation of the Optimization

The length of the first two phalanges ($l_1 + l_2$) is set to 80 mm and the fingertip length is 30 mm. Therefore, the total length of the finger is close to a human middle finger. The pulley radii r_1 and r_4 are set to 7.5 mm, which is the largest radius allowed by the mechanical design of the phalanges. To achieve a maximal workspace for in-hand manipulation, the following design variables of the gripper can be optimized:

- w_p: Width of the palm, which is measured between the two proximal finger joints
- l_1: Length of the proximal phalanges; l_2 is then given by $80 - l_1$
- r_2: Radius of the flexor pulleys at the middle joints
- r_3: Radius of the extensor pulleys at the proximal joints
- k: Stiffness of the extension springs
- α: Offset of the proximal phalanx, measured from the x-axis

As the in-hand manipulation workspace is object-dependent, in this research we optimize the workspace of manipulating the 25 mm wooden cube, as shown in Fig. 1 and 3. A position of the cube can be considered inside the in-hand manipulation workspace only if the hand–object system satisfies the following two sets of criteria.

1) Kinematic Criteria: The position of the object should lead to a feasible inverse kinematics solution. Additionally, every finger joint angle is between its joint limits and collisions between the links are avoided.

- The object position should lead to a real solution to Eqns. (6) and (7).
- In this study, the joint angles are between 0 and the joint limits (set to $2\pi/3$):

$$0 < \theta_i \leq 2\pi/3, i = 1, 2, 3, 4 \tag{16}$$

- To avoid collision of the links of the proximal parallelogram, as shown in Fig. 4(a), the angles should satisfy:

$$\alpha + \theta_1 \leq 7\pi/8 \tag{17}$$

Similarly, for the distal parallelogram:

$$\alpha + \theta_1 + \theta_2 \leq 7\pi/8 \tag{18}$$

The limit $7\pi/8$ was decided according to the CAD model of the finger. Similar constraints apply to the right finger, as θ_1 and θ_2 in the above two equations should be replaced with θ_3 and θ_4, respectively.

2) Kinetostactic Criteria: The gripper and the cube should maintain static equilibrium. Particularly, the sliding and rotation of the cube should be prevented.

- Actuation tendon forces solved by Eqns. (14)–(15) should be lower than 70 N, which is the maximal output of the adopted low-cost servo.

$$f_i \leq 70, i = 1 \text{ or } 3 \tag{19}$$

- To avoid the sliding between the fingertips and the cube, the contact force should fall within the friction angle

$$\left\| \frac{F_{Ly}}{F_{Lx}} \right\| \leq \mu \tag{20}$$

where F_{Lx} and F_{Ly} are the normal and tangential components of $\mathbf{F}_L$, respectively. Silicone rubber will be adopted at the fingertips to increase friction, and the friction coefficient μ is set to 0.5 according to [26].

- The rotation of the cube about its edges should be avoided. For example, to avoid the rotation about Point-M the contact force should fall within the angle $\angle$MPN, as shown in Fig. 4(b). This constraint can be written as:

$$\left\| \frac{F_{Ly}}{F_{Lx}} \right\| \leq 1 \tag{21}$$

- The contact force between the object and the fingertips should be large enough to resist moderate disturbance. In this optimization we set

$$F_{Lx} \geq 2 \tag{22}$$

The in-hand manipulation workspace can be numerically calculated by the following steps. An area ($-150 \leq x \leq 150, 0 \leq y \leq 150$) is discretized by a suitable step size (e.g., 2 mm). Each point in this area is set as a position of the object and is plugged into Eqn. (6) and (7) to solve the joint angles of the gripper. Then the contact force and the tendon actuation forces are solved using Eqns. (14)–(15). The solution is then checked by the kinematic and kinetostatic criteria presented above. Each point that satisfies the criteria represents an area (e.g., 4 mm^2 for the 2 mm discretization) of the in-hand manipulation workspace. Then the total area of the workspace can be calculated by counting all the qualified points.

B. Optimization Using Simulated Annealing

The simulated annealing algorithm [27], which mimics the annealing of metals, was adopted to solve the optimization.

The flowchart of the algorithm is shown in Fig. 5. At the beginning, an initial design was generated within the range of the design variables listed in Table I. The workspace is calculated using the method presented in Subsection III-A. The initial design and the corresponding workspace are set as the best design and the largest workspace, respectively. Considering the computation speed, the step size of discretization for calculation of workspace was set to 2 mm.

Mimicking the temperature decrease in annealing of metals, the algorithm decreases the temperature T by β at each iteration,

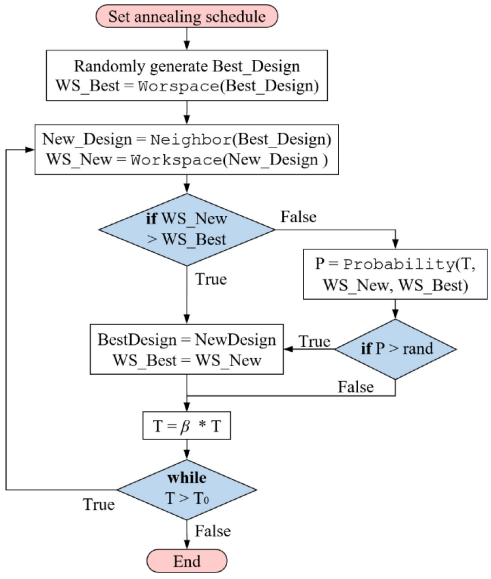

Fig. 5. The flowchart of the SA algorithm.

TABLE I
RANGE OF DESIGN VARIABLES AND OPTIMIZATION RESULTS

Variables	Range	1st trial	**2nd trial**	3rd trial	Unit
w_p	[20, 150]	42.34	**42.34**	42.74	mm
l_1	[20, 60]	40.10	**39.99**	40.04	mm
r_2	[3, 7.5]	7.21	**5.99**	6.72	mm
r_3	[3, 7.5]	3.98	**6.47**	4.94	mm
k	[0.1, 2]	1.35	**1.22**	1.50	N/mm
α	[π/8, π/2]	0.398	**0.393**	0.393	rad
Workspace (calculated by 2 mm discretization)		2672	**2672**	2672	mm^2
Workspace (re-calculated by 1 mm discretization)		2524	**2545**	2525	mm^2

until the final temperature T_0 is reached. At each temperature, a new design is generated near the best design. The distance of the new design from the best design is based on a probability distribution with a scale proportional to the temperature. If the new design gives larger workspace than the best design, the new design will be unconditionally accepted as the best design. If the new design gives smaller workspace, the design will be accepted with a probability calculated based on the temperature and the degradation of workspace. Generally, higher temperature and less degradation of workspace gives higher probability of acceptance. By accepting the designs diminishing the workspace, the algorithm avoids being trapped in local optima. Thus it is able to explore globally for more possible solutions. As the temperature decreases, the algorithm reduces the extent of its search of new designs to converge to a maximum. Additionally, the probability of accepting a worse design is also decreased.

The parameters of the algorithm were manually tuned using a trial-and-error technique, until the algorithm gives a stable result. As shown in Table I, the maximal workspace resulted in 2672 mm^2 after three consecutive computations, suggesting that the algorithm gives a stable solution. Although the areas of workspace given by three computations are the same, the three designs are slightly different from each other, suggesting that the 2 mm step size was not fine enough to differentiate the workspaces given by the three different designs. Thus, we re-calculated the workspaces of the three designs with a 1 mm discretization. The design given by the second trial is chosen as the best design, since the workspace is 2586 mm^2 which is the highest among them.

Using the optimal parameters, the manipulation workspace and actuation space of the ParaGripper manipulating the 25 mm cube is visualized in Figs. 6(a) and (b), respectively. The manipulation workspace spans 134 mm and 40 mm on $x-$ and $y-$direction, respectively. Five points are indicated on both the workspace and the actuation space, to show the correspondence between the two spaces. The contact force is also simulated and visualized in Fig. 6(a). The magnitude of contact force is indicated by the color bar while the direction of force is represented by the short red lines. As shown in Fig. 6(a), the contact force is position-dependent. The force is more normal near the center line ($x = 0$) of the workspace and the magnitude is larger at the central–bottom area of the workspace. Additionally, according to the simulation, the maximal angle of the contact force is 26.1° (measured from the $x-$axis), which is slightly smaller than the friction angle (26.6° by $\mu = 0.5$).

C. Design of the Gripper

The ParaGripper was designed as shown in Fig. 7, using the optimal parameters listed in Table I. The design is self-contained and lightweight (337 g), to facilitate further integration to a hand–arm manipulation system. The gripper is composed by off-the-shelf components and 3D-printed parts. The white parts (e.g., the phalanges, the fingertips and the pulleys) are printed with Somos GP plus resin, while the black (the palm) is FS3300PA Nylon. In addition, the contact surfaces of the fingertips are covered with silicone rubber sheet to increase friction. Two servo motors (FS5323 M by FEETECH RC Model Co. Ltd., China) are adopted. The flexor tendons are anchored to the capstans that are mounted on the servos. Two extension springs are connected to the extensors to open the finger joints. An Arduino Nano is adopted to receive commands from a PC and control the servos accordingly.

IV. EXPERIMENTAL CHARACTERIZATIONS

To evaluate the effectiveness of the proposed design, grasp and in-hand manipulation experiments have been conducted.

A. Grasp Experiments

The grasp capability of the gripper has been evaluated using the YCB object set [28]. Following the *Gripper Assessment Protocol* [28], we adopted the following objects:

- Spherical objects: Soccer ball, softball, tennis ball, racquetball, golf ball and marbles, with the diameter varying from ϕ125 mm to ϕ18 mm

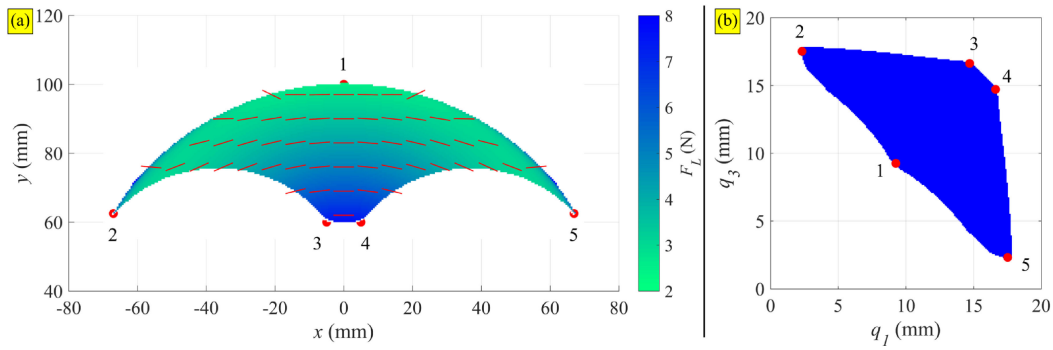

Fig. 6. (a) The simulated workspace of the gripper manipulating the 25 mm cube. The contact force magnitude is indicated by the colorbar, while the red lines represent the directions of the contact force. The Point 1∼5 indicate five representative positions within the workspace. (b) The actuation space of the gripper manipulating the 25 mm cube, with Point 1∼5 indicated.

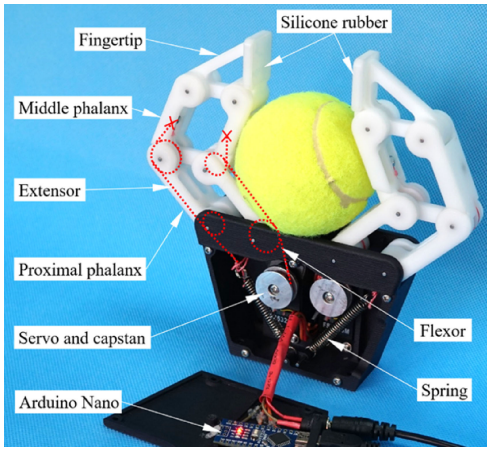

Fig. 7. Design of the ParaGripper.

- Flat objects: Washers (the thickness ranges from 1.4 mm to 3.8 mm while the diameter is between ϕ10 mm and ϕ60 mm) and credit card
- Tools: Pen, scissors, screwdriver, driller, hammer and four different sizes of clamps
- Articulated objects: Plastic chain and rope

The gripper could successfully pick up and hold every object from a desk, as some of the grasps are shown in Fig. 8(a)–(h). For big objects, the gripper could perform power grasps, which involves multiple phalanges, as shown in Fig. 7 and Fig. 8(a) and (e). For small objects, the gripper could perform pinch grasps using only the fingertips, as shown in Fig. 8(b), (c), (d), (f), (g) and (h).

The grasping force was measured by the experimental setups shown in Fig. 8(i) and (j). Following the setups in [10], [29], a commercial force sensor (ATI Nano 17 F/T) was installed inside a ϕ65 mm split cylinder and a 30 mm split cube for the force measurement of power grasp and pinch grasp, respectively. The measured power grasp force is 28.4 N, while the pinch grasp force is 12.1 N. Notably, the gripper can lift 2 kg water using both power grasp and pinch grasp, as shown in Fig. 8(k) and (l) respectively, suggesting that the gripper can be used for general pick-and-place tasks.

Fig. 8. The ParaGripper grasping different objects: (a) ϕ 125 soccer ball, (b) ϕ16 mm marble ball, (c) ϕ20 mm washer, (d) credit card, (e) driller, (f) hammer, (g) clamp, (h) plastic chain, (i) ϕ65 mm split cylinder and (j) 30 mm split cube with force sensor inside, (k) 2 kg water bottle by power grasp and (l) pinch grasp.

B. *In-Hand Manipulation Experiments*

The hand was first commanded to perform in-hand manipulation of four different objects, including the 25 mm cube, the 40 mm cube, the ϕ25 mm cylinder and the ϕ40 mm cylinder shown in Fig. 9(a).

The gripper could successfully manipulate the 25 mm cube to the five points indicated in Fig. 6. Fig. 1(a)–(e) shows the cube at Point 1∼5, respectively. There is no slipping or rotation of the cube observed during the manipulation. The width and height

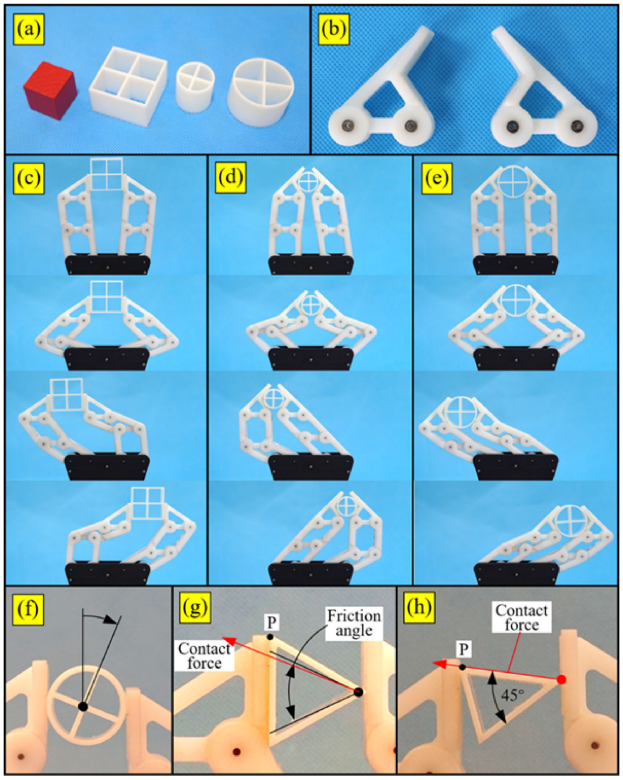

Fig. 9. In-hand manipulation experiments: (a) The objects: a 25 mm cube, a 40 mm cube, a ϕ25 mm cylinder and a ϕ40 mm cylinder. (b) Fingertips with prismatic jaw. (c) Manipulation of the 40 mm cube with parallel fingertips. (d) Manipulation of the ϕ25 mm and (e) the ϕ45 mm cylinder with the prismatic fingertips. (f) Manipulation of the ϕ25 mm cylinder with the parallel fingertips. (g) Manipulation of an equilateral triangle and (h) an isosceles triangle with 45° vertex angle using the parallel fingertips.

TABLE II
THE WIDTH AND HEIGHT OF IN-HAND MANIPULATION WORKSPACE

Object	Width	Height
25 mm cube	141 mm	41.3 mm
40 mm cube	91 mm	38.7 mm
ϕ25 mm cylinder	89 mm	39.6 mm
ϕ40 mm cylinder	137 mm	39.6 mm

of the manipulation workspace, measured from the snapshots, is 141 and 41.3 mm respectively. The measured result is slight larger than the simulation result shown in 6, possibly due to the manufacturing error of the components.

Snapshot sequences of the manipulation of the 40 mm cube, the ϕ40 mm cylinder and the ϕ 25 mm cylinder are shown in Fig. 9(c), (d) and (e), respectively. With different objects, the manipulation workspace changes. The widths and heights of the workspaces are listed in Table II . To manipulate the cylinders, the parallel fingertips were replaced by the fingertips with prismatic jaws, as shown in Fig. 9(b). Since there are no tendons connected to the fingertips, it is easy to change the fingertips. Similarly to previous manipulation experiments, the objects was manipulated to the edge of the manipulation workspace. During the manipulation, the prismatic jaws stably hold the cylinders, although the shape of the jaws was not numerically optimized.

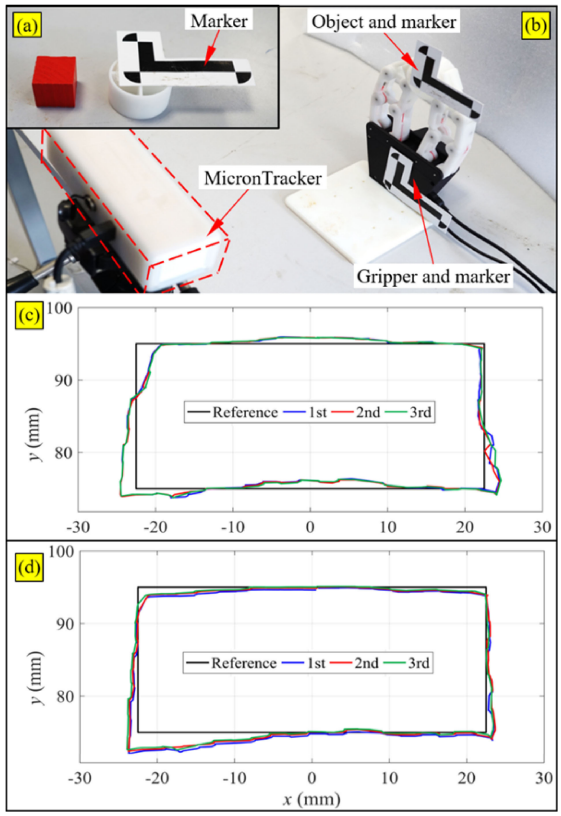

Fig. 10. In-hand manipulation experiments: (a) The 25 mm wood cube and the ϕ 40 mm cylinder with a marker attached, (b) experimental setup of the measurements, (c) trajectory of manipulating the 25 mm cube and (d) trajectory of manipulating the ϕ40 mm cylinder.

As emphasized in Section II, the non-parasitic in-hand manipulation relies on the assumption that the object remains stationary within the fingertips. The fingertips should be designed according to the object to prevent sliding and rotation between the object and the fingertips. For example, a cylindrical object can be manipulated by a prismatic fingertip as shown in Fig. 9(d) and (e), as each fingertip provides two contact points. However, if the parallel fingertip is adopted for manipulation of the cylinder, parasitic rotation occurs as shown in Fig. 9(f).

In addition, we tested the in-hand manipulation of an equilateral and an isosceles triangular with 45° vertex angle. Both triangles have an aptitude of 25 mm, thus the contact force is the same as the 25 mm cube, as simulated in Fig. 6. According to the simulation, the maximal angle of the contact force is 26.1°. The gripper could manipulate the equilateral triangle without parasitic rotation, because the contact force falls within the 60° angle ($26.1° < 30°$), as shown in Fig. 9(g). Oppositely, for the isosceles triangle, as the contact force no longer falls within the 45° vertex angle ($26.1° > 22.5°$), the triangle was rotated, as shown in Fig. 9(h).

To quantify the manipulation accuracy, the gripper was commanded to follow a 45 mm by 20 mm rectangular trajectory when manipulating the 25 mm cube and the ϕ40 mm cylinder shown in Fig. 10(a). The experimental setup is shown in Fig. 10(b). Two markers were attached to the palm and the object. An optical tracker (MicronTracker SX60, Claron Technology

Inc.) was used to measure the positions and orientations of the markers. The measurement of the manipulation of each object were repeated for three times.

The recorded trajectories are plotted in Fig. 10(b) and (c) for the cube and the cylinder, respectively, accompanied by the reference trajectories. The change of orientation during the manipulation is less than 1.44° and 1.65° for the cube and the cylinder, respectively. The rotation may be derived from the structure elasticity of the phalanges. The silicon pad on the fingertips could be another source of the rotation. The maximal position error is 2.17 mm for manipulation of the cube and 3.16 mm for the cylinder.

V. Conclusions and Future Work

To eliminate the parasitic rotation of in-hand manipulation performed by underactuated robotic hands, this paper proposes the ParaGripper. The gripper has two underactuated fingers and each finger is composed of two serially connected parallelograms. By adopting the parallelograms and a suitable fingertip design, the orientation of the objects can be maintained during in-hand manipulation. The experiments demonstrated that with suitable fingertips the ParaGripper could in-hand manipulate different objects without parasitic rotation, while the capability of performing adaptive grasps was maintained. In view of the proven functionality, the ParaGripper is expected to be a solution for versatile manipulation tasks.

The presented non-parasitic in-hand manipulation relies on the assumption that the object remains stationary within the fingertips. The fingertips should be designed accordingly to prevent sliding and rotation of the object. A universal fingertip design accommodating different objects is an interesting direction for further investigation. In the future, the gripper will be integrated with a manipulator to form a complete hand–arm manipulation system, which is expected to offer better manipulation dexterity, as compared to conventional systems with parallel jaw grippers. The kinematics and path planning problems of the hand–arm system will also be studied.

Acknowledgment

The authors would like to thank Pasquale Ferrentino for his kind help in the testing of the ParaGripper.

References

[1] J. K. Salisbury and J. J. Craig, "Articulated hands: Force control and kinematic issues," *Int. J. Robot. Res.*, vol. 1, no. 1, pp. 4–17, 1982.

[2] M. T. Mason and J. K. Salisbury Jr, *Robot Hands and the Mechanics of Manipulation*. Cambridge, MA: MIT Press, 1985.

[3] M. Grebenstein *et al.*, "The hand of the dlr hand arm system: Designed for interaction," *Int. J. Robot. Res.*, vol. 31, no. 13, pp. 1531–1555, 2012.

[4] G. Palli *et al.*, "The dexmart hand: Mechatronic design and experimental evaluation of synergy-based control for human-like grasping," *Int. J. Robot. Res.*, vol. 33, no. 5, pp. 799–824, 2014.

[5] Z. Li, P. Hsu, and S. Sastry, "Grasping and coordinated manipulation by a multifingered robot hand," *Int. J. Robot. Res.*, vol. 8, no. 4, pp. 33–50, 1989.

[6] V. Kumar, E. Todorov, and S. Levine, "Optimal control with learned local models: Application to dexterous manipulation," in *Proc. IEEE Int. Conf. Robot. Autom.*, 2016, pp. 378–383.

[7] M. Andrychowicz *et al.*, "Learning dexterous in-hand manipulation," *Int. J. Robot. Res.*, vol. 39, no. 1, pp. 3–30, 2020. [Online]. Available: https://doi.org/10.1177/0278364919887447.

[8] F. Ficuciello, D. Zaccara, and B. Siciliano, "Synergy-based policy improvement with path integrals for anthropomorphic hands," in *Proc. IEEE/RSJ Int. Conf. Intell. Robots Syst.*, Oct. 2016, pp. 1940–1945.

[9] L. U. Odhner and A. M. Dollar, "Stable, open-loop precision manipulation with underactuated hands," *Int. J. Robot. Res.*, vol. 34, no. 11, pp. 1347–1360, 2015.

[10] L. U. Odhner *et al.*, "A compliant, underactuated hand for robust manipulation," *Int. J. Robot. Res.*, vol. 33, no. 5, pp. 736–752, 2014.

[11] N. Rojas, R. R. Ma, and A. M. Dollar, "The GR2 gripper: An underactuated hand for open-loop in-hand planar manipulation," *IEEE Trans. Robot.*, vol. 32, no. 3, pp. 763–770, Jun. 2016.

[12] R. R. Ma, W. G. Bircher, and A. M. Dollar, "Modeling and evaluation of robust whole-hand caging manipulation," *IEEE Trans. Robot.*, vol. 35, no. 3, pp. 549–563, Jun. 2019.

[13] H. Liu, Z. Zhang, X. Zhu, and K. Xu, "A single-actuator gripper with a working mode switching mechanism for grasping and rolling manipulation," in *Proc. IEEE/ASME Int. Conf. Adv. Intell. Mechatronics*, 2018, pp. 359–364.

[14] K. Xu and H. Liu, "Continuum differential mechanisms and their applications in gripper designs," *IEEE Trans. Robot.*, vol. 32, no. 3, pp. 754–762, Jun. 2016.

[15] M. V. Liarokapis and A. M. Dollar, "Post-contact, in-hand object motion compensation with adaptive hands," *IEEE Trans. Autom. Sci. Eng.*, vol. 15, no. 2, pp. 456–467, Apr. 2018.

[16] J. M. Hervé, "Group mathematics and parallel link mechanisms," in *Robotics, Mechatronics and Manufacturing Systems*. New York, NY, USA: Elsevier, 1993, pp. 57–62.

[17] L. W. Tsai and R. Stamper, "A parallel manipulator with only translational degrees of freedom," in *Proc. ASME Des. Eng. Tech. Conf.*, 1996.

[18] X. J. Liu and J. Wang, "Some new parallel mechanisms containing the planar four-bar parallelogram," *Int. J. Robot. Res.*, vol. 22, no. 9, pp. 717–732, 2003.

[19] S. Hirose and Y. Umetani, "The development of soft gripper for the versatile robot hand," *Mechanism Mach. Theory*, vol. 13, no. 3, pp. 351–359, 1978.

[20] L. Birglen and C. M. Gosselin, "Kinetostatic analysis of underactuated fingers," *IEEE Trans. Robot. Autom.*, vol. 20, no. 2, pp. 211–221, Apr. 2004.

[21] Q. Li and J. M. Hervé, "1T2R parallel mechanisms without parasitic motion," *IEEE Trans. Robot.*, vol. 26, no. 3, pp. 401–410, Jun. 2010.

[22] L. Birglen, T. Laliberté, and C. M. Gosselin, *Underactuated Robotic Hands*, vol. 40. Berlin, Germany: Springer, 2007.

[23] J. Borràs and A. M. Dollar, "Analyzing dexterous hands using a parallel robots framework," *Auton. Robots*, vol. 36, no. 1-2, pp. 169–180, 2014.

[24] A. Mo and W. Zhang, "Pin array hand: A universal robot gripper with pins of ellipse contour," in *Proc. IEEE Int. Conf. Robot. Biomimetics*, 2017, pp. 2075–2080.

[25] E. Brown *et al.*, "Universal robotic gripper based on the jamming of granular material," *Proc. Nat. Acad. Sci.*, vol. 107, no. 44, pp. 18809–18814, 2010.

[26] Engineers Edge LLC, "Coefficient of friction equation and table chart," Engineers Edge, 2018. [Online]. Available: https://www.engineersedge.com/coeffients_of_friction.htm, Accessed: Mar. 7, 2018.

[27] S. Kirkpatrick, C. D. Gelatt, and M. P. Vecchi, "Optimization by simulated annealing," *Science*, vol. 220, no. 4598, pp. 671–680, 1983.

[28] B. Calli, A. Walsman, A. Singh, S. Srinivasa, P. Abbeel, and A. M. Dollar, "Benchmarking in manipulation research: Using the Yale-CMU-Berkeley object and model set," *IEEE Robot. Autom. Mag.*, vol. 22, no. 3, pp. 36–52, Sep. 2015.

[29] J. A. Falco, K. Van Wyk, and E. R. Messina, "Performance metrics and test methods for robotic hands," Special Publication (NIST SP) - 1227 (Draft), Tech. Rep., 2018.